Ion-beam-driven warm dense matter experiments

F.M. Bieniosek[1,2], J. J. Barnard[1,3], A. Friedman[1,3], E. Henestroza[1,2], J. Y. Jung[1,2], M. A. Leitner[1,2], S. Lidia[1,2], B. G. Logan[1,2], R. M. More[1,2], P. A. Ni[1,2], P. K. Roy[1,2], P. A. Seidl[1,2], W. L. Waldron[1,2]

[1]*HIFS-VNL*

[2]*LBNL, Berkeley, CA, USA*

[3]*LLNL, Livermore, CA, USA*

E-mail: fmbieniosek@lbl.gov

Abstract. As a technique for heating volumetric samples of matter to high energy density, intense beams of heavy ions are capable of delivering precise and uniform beam energy deposition dE/dx, in a relatively large sample size, and with the ability to heat any solid-phase target material. The US heavy ion fusion science program has developed techniques for heating and diagnosing warm dense matter (WDM) targets. The WDM conditions are achieved by combined longitudinal and transverse space-charge neutralized drift compression of the ion beam to provide a hot spot on the target with a beam spot size of about 1 mm, and compressed pulse length about 2 ns. Initial experiments use a 0.3 MeV, 30-mA K+ beam (below the Bragg peak) from the NDCX-I accelerator to heat foil targets such as Au, Al and Si. The NDCX-1 beam contains an uncompressed pulse up to >10 μs of fluence ≥200 kW/cm2, and a compressed pulse of fluence ~10 mJ/cm2. This beam heats 150-nm Au targets to above 3000 K.

We have developed a WDM target chamber and a suite of target diagnostics including a fast multi-channel optical pyrometer, optical streak camera, VISAR, and high-speed gated cameras. The optical target emission spectrum is measured by a high dynamic range Hamamatsu streak camera coupled with a spectrometer. Initial WDM experiments heat targets by both the compressed and uncompressed parts of the NDCX-I beam, and explore measurement of temperature, droplet formation and other target parameters. Continued improvements in beam tuning, bunch compression, and other upgrades are expected to yield higher temperature and pressure in the WDM targets. Future experiments are planned in areas such as dense electronegative targets, porous target homogenization and two-phase equation of state.

*This work was performed under the auspices of the U.S Department of Energy by Lawrence Livermore National Laboratory under Contract DE AC52 07NA27344, and by the University of California, Lawrence Berkeley National Laboratory under Contract DE AC03 76SF00098.

1. Introduction

The US heavy ion fusion science program is developing techniques for heating ion-beam-driven warm dense matter (WDM) targets [1-4]. Intense ion beams have several attractive features as a technique for generating WDM. These features include:

-Precise control of local beam energy deposition dE/dx, nearly uniform throughout a given volume, and not strongly affected by target temperature,

-Large sample sizes (about 1 micron thick by 1 mm diameter),

-The ability to heat any target material, for example, foams, powders, conductors, insulators, solid, gas, etc.

The WDM conditions are achieved by combined longitudinal and transverse space-charge neutralized drift compression of the ion beam to provide a hot spot on the target with a beam spot size of about 1 mm, and compressed pulse length about 2 ns. The experiments use a 0.3 MeV, 30-mA K+ beam (below the Bragg peak) from the NDCX accelerator to heat foil targets such as Au, Al and Si. The NDCX beam contains an uncompressed pulse length up to 20 μs with a peak energy flux >100 kW/cm2, and a compressed pulse of fluence ~10 mJ/cm2.

We have recently improved the NDCX beamline and its capabilities for WDM studies. The improvements derive from the replacement of the original Induction Bunching Module (IBM) with a new one that can generate nearly twice the volt-seconds, and from a longer neutralized drift section that allows the longer duration energy modulated pulses to fully compress at the target plane. The IBM waveform has been optimized for several operating beam energies. The waveform fidelity is such that the relative error in energy is less than 1% over ~400-500 ns pulse duration.

The temporal profile of the beam current is measured with a Faraday cup at the target plane that has ~1 ns response time. The beam energy is scanned to find the optimum operating conditions that produce the highest peak current and compressed pulse power and deposited energy. A secondary scan of the final matching solenoid field strength is performed to optimize the beam intensity and compressed pulse beam fluence.

2. Target positioner and diagnostics

The target holder has two axes of motor drives to provide two degrees of freedom of remote positioning of the target. These include 2 axes on the target positioner and 2 axes on the light collection optics table. This configuration allows us to remotely position the target and target assembly without breaking vacuum to move the target to an undamaged spot. The target contains a set of improved fiducials and alignment aids for speeding up the process of alignment of the target and light collection optics. The precision target positioning equipment allows rapid re-positioning of the target foil between shots. Using this positioning equipment, we have been able to reduce the shot-to-shot repetition time to as little as 4 minutes. Fig. 1 shows a platinum target after a number of shots were taken on the foil. The target manipulator was used to reposition the target between shots. Up to 40 beam shots were taken per day with a repetition rate of as little as 4 minutes. A total of 69 beam-target shots were taken using this foil before it was removed from the target chamber and replaced with a fresh foil.

Fig. 1. Target holder containing a platinum target foil (above) and a small scintillator (below).

Target diagnostics [4] include a fast optical pyrometer, an optical streak-spectrometer, VISAR, and two high-speed gated image intensified cameras. We have installed a new current monitor downstream of the target. This current monitor is a Bergoz FCT-016-20:1-VAC fast current transformer with a 20:1 turns ratio. The purpose of the current monitor is to measure beam current transmitted through the target as a function of time. In a target thicker than the range of the beam, the beam current transmitted should be small even as the target vaporizes since the beam stopping for solid and vapor target material is very similar. This is the case if no droplets form in the target. However if and when the target bunches up into droplets we expect to see a change in transmitted beam current.

Improvements to the target assembly include the installation of a simple final focus cone. The cone has a 4-mm entrance aperture, 1-mm exit aperture, and a pitch angle of 200 mrad. The cone enhances beam intensity on target by reflecting additional beam ions that are initially radially outside the target area. In addition to enhanced flux, other expected advantages of the cone include: 1. An additional source of electrons from ion collisions with the cone for space charge neutralization at the target; 2. Reduced beam space potential because of the close proximity of the metal cone wall to the beam; and 3. Improved uniformity of beam energy flux on target because of the presence of reflected ions among the beam ions striking the target.

3. Model of target dynamical response

As the ion beam deposits the energy volumetrically on the solid target, the target goes through a series of phase changes depending on the total beam energy fluence and power. For the beam power density levels available in NDCX-1, in the 100 kW/cm^2 range for the longitudinally uncompressed beam (for several μs), and in the >> 1 MW/cm^2 range for the longitudinally compressed beam (for 2 ns) the target will go through a melting process and vaporize a fraction of its mass reaching temperatures near 0.5 eV (~ 6000 K).

NDCX-1 can compress the beam spot size to a radius of about 1 mm. The targets are thin foils less than a micron in thickness. The diffusivity of these targets of order 1 cm^2/s or less, which means that even for the 10-μs pulse time scale the heat diffuses transversely by less than 30 microns. Therefore we can model the target dynamics using only time and the spatial dimension along the beam direction. The equation of heat conduction for the temperature T(x,t) is

$$\rho c_p \frac{\partial T}{\partial t} = \frac{\partial}{\partial x}\left(K \frac{\partial T}{\partial x} \right) + S(x,t),$$

where ρ, c_p and K are the density, the specific heat at constant pressure, and thermal conductivity which may be functions of temperature and position; S(x,t) is an external source of heat which in our

case is the heat generated by the ions deposited in the target. The initial condition is $T(x,t=0) = T_0$ where $T_0 = 293$ K. The boundary condition on the surface of the foil (both sides) is given by

$$\left(K\frac{\partial T}{\partial x}\right)_{L,R} = F_{L,R}(T),$$

where $F_{L,R}$ is the (left and right) energy flux off the surface of the foil due to evaporation, radiation, and thermionic (Richardson) emission; Joule (resistive) heating from the electron current is neglected. Note that $F_R=-F_L$□$F(T)= Fv(T)+Fr(T)+Ft(T)$ and that the boundary is moving because the foil evaporates continuously.

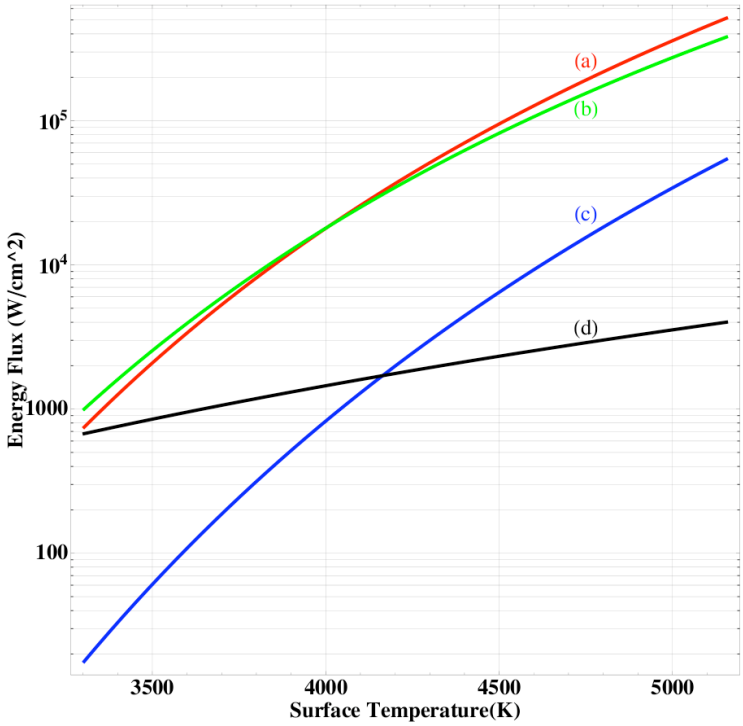

Fig. 2. Energy flux from cooling mechanisms in the equilibrium model for Pt.

Figure 2 shows the relative importance of each of the cooling mechanisms as a function of surface temperature. Curve (a) corresponds to the energy flux from evaporation as calculated using data from the CRC tables; curve (b) is also the energy flux from evaporation but calculated using the Clausius-Clapeyron equation; curve (c) corresponds to the energy flux from Richardson cooling; and curve (d) is the energy flux thermal radiation.

Using this model we calculate the temperature at which the cooling mechanisms equilibrate the energy flux from the ion beam (Fig. 2). NDCX-I delivers beam intensity sufficient to reach equilibrium temperatures in the range of 3000 to 6000 K.

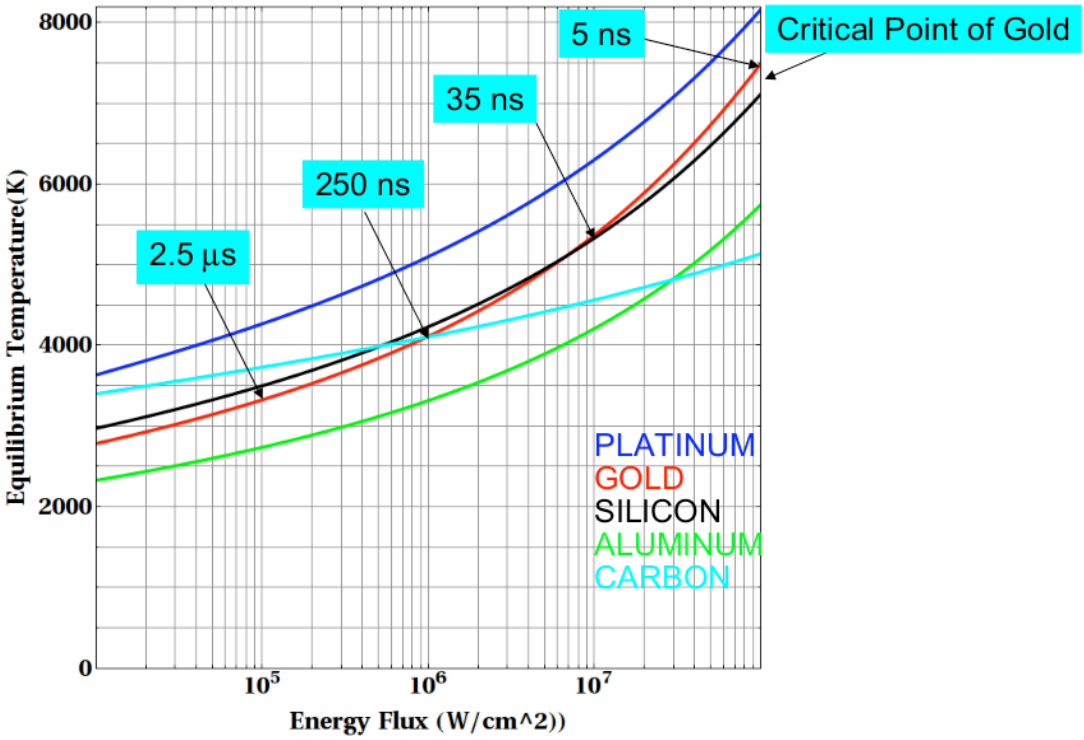

Fig. 3. Equilibrium temperature as a function of beam energy flux. Times indicated refer to time needed to reach equilibrium temperature.

The target temperature reaches an equilibrium within a time on the order of 1 μs. The temperature then slowly falls as the target becomes thinner due to vaporization from the front and rear surfaces. The calculation is based on the energy deposition model of the TRIM code. The thickness of each target is: Gold: 150 nm, Aluminum: 350 nm, Platinum: 120 nm, Silicon: 400 nm, and Carbon: 400 nm.

One of the key areas of investigation in warm dense matter is the dynamic transition between liquid and vapor of superheated metals. In particular, as the solid is heated above the melting temperature it first enters a liquid state (or if the temperature is high enough -- above the critical point-- it enters a fluid state that could be considered either liquid or vapor). In NDCX I, the temperature reached in metals such as gold and aluminum places it in a liquid state. As discussed above, the foil reaches a quasi-equilibrium, which is a balance between heating by the beam and cooling by evaporation and electron emission. As the pressure builds in the foil, expansion will occur, and droplets will form, due to surface tension effects. A complete theory of precisely how these droplets form is lacking but we have physical arguments and quantitative estimates that suggest that they should form. We have experimental evidence for droplet formation from three independent optical measurements:
1. The first indication that droplets form comes from the intensity measurements of the gold foil. During beam heating of the foil, after approximately 2 μs, the light intensity begins to decrease. One explanation for this effect is the reduction in projected surface area, as the ~200 nm foil breaks up into ~ 1000 nm radius droplets. The reduction in light intensity corresponds to the reduction in projected surface area.
2. The most direct measurement of the droplets, are photographic images of several hundred point sources of light expanding at a speed of a few meters/sec, that have been obtained from the Au and Pt foils. Although the size of the droplets is below the resolution of the camera, if we assume the mass of

the heated part of the foil is converted into droplets, then the quantity of droplets implies that size of the droplets is on the order of a micron.
3. The third area of evidence is the dynamic change in the spectrum of the foil. Roughly at the time that the intensity decreases (after ~ 2 or 3 μs) the intensity at wavelengths longer than about 600 nm begins to decrease, whereas the intensity below that wavelength remains constant. If the droplets are smaller than the wavelength of light they will be poor radiators, and so the wavelength at which the spectrum begins to turn over is an indicator of the droplet scale size. Not all of the targets tested, have been observed to display all of these characteristics.
4. A fourth area of evidence is based on preliminary analysis of the current transformer data. The current transformer shows a rapid increase in signal level at about 2 μs into the beam pulse, suggesting breakup of the target into droplets at about this time. When the target bunches up into droplets, much of the incident beam current can pass through the target to be detected by the current transformer downstream of the target.

We are beginning to compare detailed theory that describes the emission spectrum from droplets. We use handbook values for the room-temperature optical constants and assume these do not change significantly at the temperature of the experiments. The calculation is done by extending the textbook Mie scattering theory to a general dielectric function and adapting it to calculate absorption and emission coefficients for the droplets. For droplets at a radius of 0.1 micron the emission has qualitative features suggestive of the data (including the decreased emission at long wavelengths). However, at a droplet radius of 0.2 microns the spectrum is quite different, suggesting that these spectral measurements may be sensitive indicators of droplet size. This work is in progress.

4. Experimental beam-target data

NDCX-I beam-target shots have been performed on gold, platinum, carbon, aluminum and silicon targets. Typical experimental results for some of these targets are described below. Optical data was taken using gated ICCD cameras, the streak spectrometer, and the fast optical pyrometer diagnostic. Reconstructed temperature, T, is obtained from non-linear least square fit of experimental spectra, I(λ,T) to a radiation model. The model is the Planck formula multiplied by emissivity, ε(λ,T), which is depending on situation, has either linear or square dependence on wavelength [5].

$$I(\lambda, T) = \varepsilon(\lambda) \cdot \frac{C_1}{\lambda^5} \frac{1}{e^{\frac{C_2}{\lambda T}} - 1}.$$

The streak-spectrometer data indicates that the target temperature in platinum reaches >4000 K, in approximate agreement with model predictions. Fig. 4 shows typical streak-spectrometer data for the platinum target temperature. Note that the measured target temperature remains slightly lower than the predicted temperature. Rapid changes in target emissivity again account for differences in the brightness temperature and corrected temperature. In contrast to the Au data (below) there are no strong emission lines in the visible range for Pt vapor.

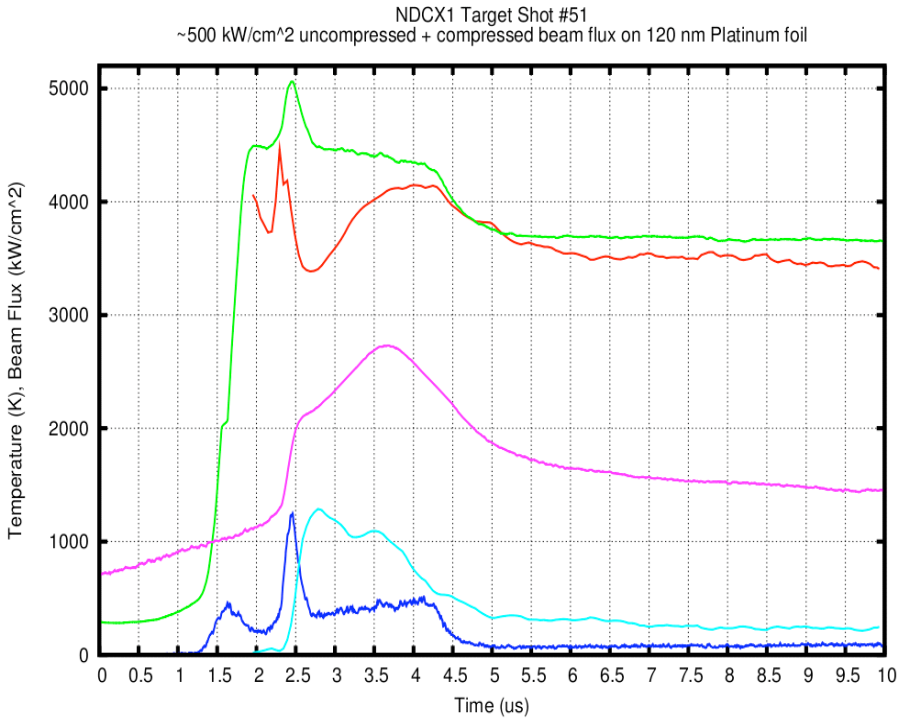

Fig. 4. Reconstructed target temperature (red) using a fit to the measured emissivity curve, brightness temperature (magenta), emissivity at 600 nm (blue), and relative time history of beam intensity (blue). The compressed pulse is timed at 1 μs after the head of the beam. Also shown is the predicted temperature behavior from the equilibrium model (green) based on the beam current pulse shown.

Fig. 5 shows optical self-emission from the expanding shower of hot debris (liquid droplets) 500 μs after the platinum target shot. The presence of hundreds of hot droplets supports the characterization of the target as forming droplets early in the beam pulse.

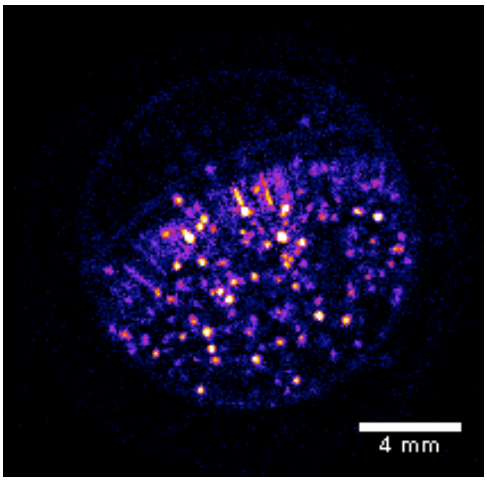

Fig. 5. Shower of hot debris (droplets) 500 μs after the beam pulse.

The evolution of the Au target during and after the ion-beam-heating can be characterized by 3 distinct phases.

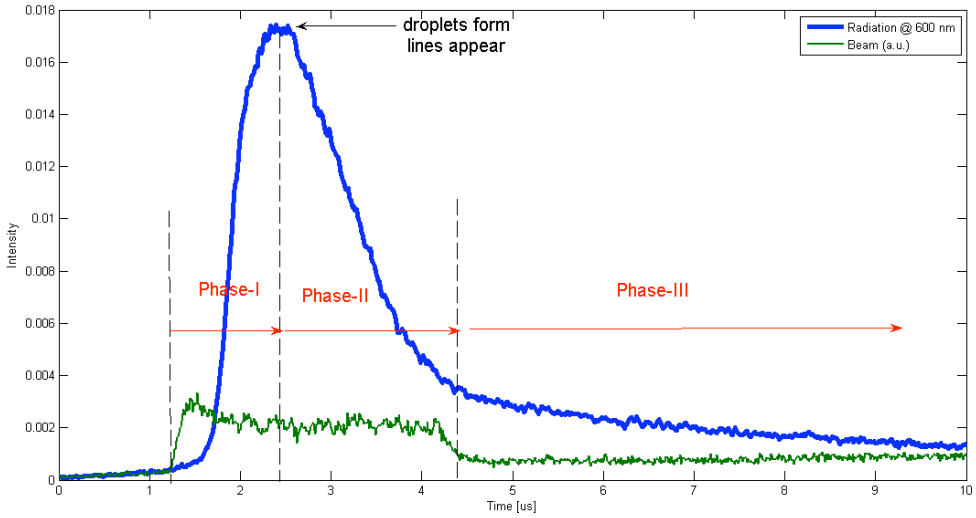

Fig. 6: Thermal radiation at 600 nm and heating-ion-beam intensity .

Under a continuous heating rate the thermal radiation reaches maximum after about 1.5 μs relative to the head of the beam (Figure 6, Phase 1). Since the ion beam is turned off later (5 μs), one would naturally expect radiation to remain at a high level during the beam pulse. This would be true if the sample remained intact during the entire heating process. However in the case of thin foils, the disassembly of a foil into droplets results in an early peak in radiation pattern. The peak in pyrometer records can be used for timing of foil disassembly.

Phase 2: Au lines appear in spectral records slightly after the radiation peaks . All gold lines were identified as Au I (atomic vapor), Fig. 7. The foil is transformed into droplets flying apart with ever increasing void. This effectively means a decrease of radiating surface area within the field of view of the diagnostic, resulting in overall decreasing of signal. Note that, while overall radiation decreases, the reconstructed temperature (from fit), gives either a constant temperature or a slight increase (beam still deposits energy into droplets), Fig. 8. This is reasonable since the cooling of droplets proceeds slowly at μs time scales, and therefore temperature of droplets is effectively "locked in" and corresponds to the peak temperature before the foil disassembly.

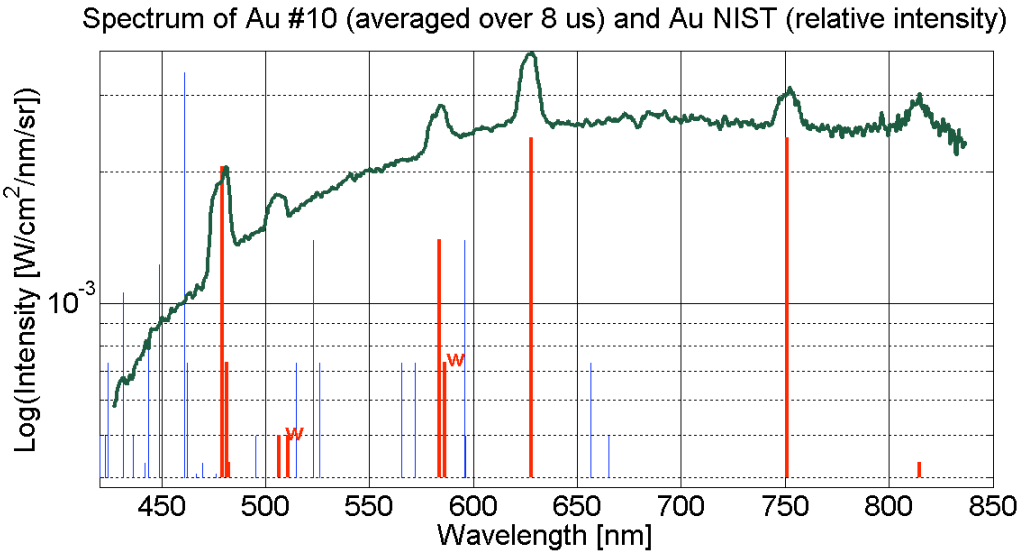

Fig. 7: Au I lines (from NIST tables) atop the continuous radiation emanating from liquid gold droplets indicate the presence of both liquid and vapor states.

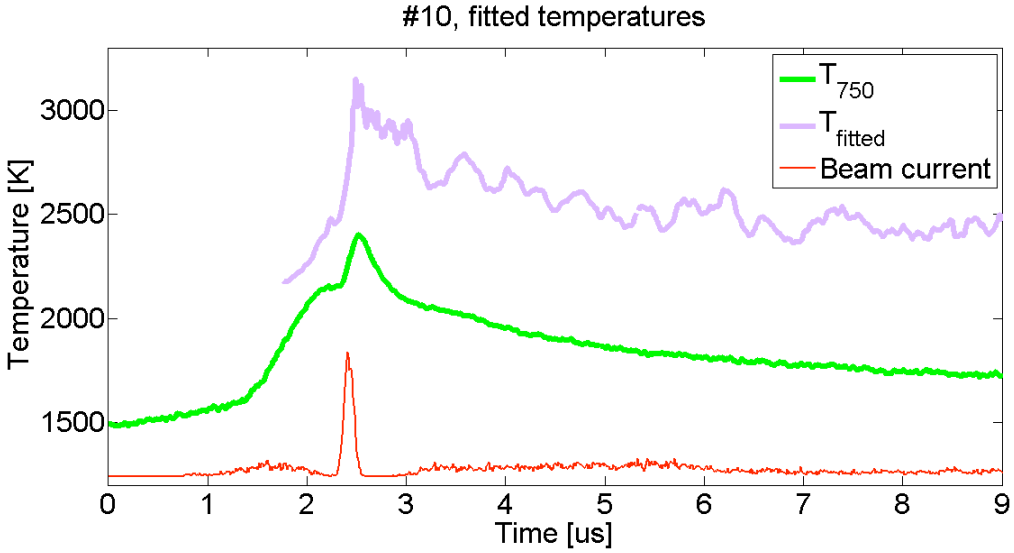

Fig. 8: Temperature reconstruction shows constant temperature after the breaking of the foil, while intensity of radiation alone decreases.

Phase 3: The radiating droplets fly apart from the field of view (400 μm circle), and the signal decreases. At later times only droplets with velocity vectors initially lying within the light collection optics aperture (22 deg) remain and therefore a nearly constant signal, i.e. "locked temperature" is detected, see Figure 8. The presence of atomic lines confirms presence of gaseous Au. This in turns leads to conclusion that the heating beam is sufficiently powerful to partially vaporize the Au sample.

Since the thickness of the Au target is larger than the range of ions, most of the ions are stopped in the target. Since the lines are ion-beam-pumped, then the moment the lines appear is clearly related to breaking of the foil, i.e. ions now can pass through the void and excite the Au vapor downstream of the target.

5. Conclusions

Rapid bulk heating of target foils to temperatures up to ~4500 K (0.4 eV) has been achieved using NDCX-I beams. The mechanism of target heating is described by a simple model which indicates the equilibrium between energy input from the beam and energy loss from the surface of the target due to mechanisms such as vaporization of the target material. Development of techniques for heating and diagnosing targets opens up the field of bulk heating of WDM targets in the laboratory using ion beam heating. The NDCX-I environment is conducive to multiple repetitive target experiments for detailed study of target behavior under various conditions and using multiple diagnostics.

Evidence for the formation of liquid metal droplets on the μs time scale is presented, and compared with predictions. Further experimental and theoretical work is underway in this area to improve our understanding of the mechanisms of droplet formation. The liquid-vapor transition region, and the formation of droplets is a matter of interest in WDM equation of state studies. Our experiments are expected to shed light on droplet formation in metal targets under WDM conditions and on the properties of the subsequent debris shower. These results could find wide application in areas such as simulating volumetric neutron heating in inertial confinement fusion experiments, and other applications of liquid metal droplets.

Other future areas of study include the equation of state near the solid-liquid and liquid-vapor phase boundaries, and material properties such as the evaporation rate, surface tension, electrical conductivity; porous targets; positive ion/negative ion experiments in high electron affinity targets; etc.

The NDCX I work is essential to benchmarking our beam manipulation, targetry, and diagnostic techniques for NDCX II, which will be able to probe the WDM regime at higher temperatures and pressures. Improvements to the beamline, targetry and diagnostic components will continue to be made to improve the facility for a variety of WDM experiments.

6. References

1. B.G. Logan, et al., Heavy ion fusion science research for high energy density physics and fusion applications, IFSA 2007, Journal of Physics, Conference Series 112 (2008) 032029.
2. J.J. Barnard, et al., Accelerator and ion beam tradeoffs for studies of warm dense matter, Proc. 2005 Particle Accelerator Conference, p. 2568
3. P.A. Seidl, A. Anders, F.M. Bieniosek, J.J. Barnard, J. Calanog, A.X. Chen, R.H. Cohen, J.E. Coleman M. Dorf, E.P. Gilson, D. P. Grote, J.Y. Jung, M. Leitner, S.M. Lidia, B.G. Logan, P. Ni, P.K. Roy, K. van den Bogert, W.L. Waldron, D.R. Welch, Progress in beam focusing and compression for warm-dense-matter experiments, Nucl. Instrum. Meth. A 606 (2009) 75-82.
4. F.M. Bieniosek, E. Henestroza, M. Leitner, B.G. Logan, R.M. More, P.K. Roy, P. Ni, P.A. Seidl, W.L. Waldron, J.J. Barnard, High energy density physics experiments with intense heavy ion beams, Nucl. Instrum. Meth. A 606 (2009) 146-151.
5. P.A. Ni, M.I. Kulish, V. Mintsev, D.N. Nikolaev, V.Ya. Ternovoi, D.H.H. Hoffmann, S. Udrea, A. Hug, N.A. Tahir, D. Varentsov, “Fast six-channel pyrometer for warm-dense-matter experiments with intense heavy-ion beams”, Laser and Particle Beams, December 2008.